Journal of Physics: Conference Series **2156** (2022) 012080 doi:10.1088/1742-6596/2156/1/012080

Superconducting thin film spiral coils as low-noise cryogenic actuators

E.C. Ferreira[1], F. Bocchese[2], F. Badaracco[1], J.V. van Heijningen[1], S. Lucas[2,3], A. Perali[4]

[1]Centre for Cosmology, Particle Physics and Phenomenology (CP3), Université catholique de Louvain, 1348 Louvain-la-Neuve, Belgium
[2]Laboratoire d'Analyse par Reaction Nucléaire, University of Namur, 61 Rue de Bruxelles, 5000 Namur, Belgium
[3]Innovative Coating Solutions (ICS), 11 Place Saint Pierre, 5380 Forville, Belgium
[4]School of Pharmacy, Physics Unit, SuperNano Laboratory, University of Camerino, 62032 - Camerino (MC), Italy

E-mail: elvis.camilo@uclouvain.be

Abstract. We present results on actuator development for a cryogenic superconducting inertial sensor with a displacement sensitivity of a few fm/$\sqrt{\text{Hz}}$ at 0.5 Hz. The first version will use niobium as sensor mechanics material. Niobium is sufficiently superconducting below 5 K allowing superconducting coils to form low-noise actuators as part of a force feedback sensing scheme. Future improvements include the use of silicon in combination with high temperature superconductors for even lower frequency fm/$\sqrt{\text{Hz}}$ performance. This device will be the world's most sensitive low-frequency inertial sensor. Here, we focus on its actuator, which ensures low-noise performance below 5 Hz by decreasing the mechanical loss and therefore thermal noise.

1. Introduction

With the first detection of gravitational waves (GWs) [1], the most precise distance measurement ever was made. The first coincidental measurement of GWs with electromagnetic counterparts, GW170817, from a binary neutron star merger [2, 3] subsequently started the new field of multi-messenger astronomy. All these monumental measurements would not have been possible without attenuating the Earth's ever-present motion coupling to the mirrors of the detectors. The inertial sensors used in GW detectors are mostly commercial, *e.g.* the Sercel L4C [4] or the Geotech GS13 [5], but some custom built accelerometers have been developed, *e.g.* in Virgo's super attenuators [6]. Recently, an interferometric readout [7] has been combined with a monolithic accelerometer [8] at Nikhef. Measurements were performed using a prototype [9]. Note that low frequency performance is subject to angular-to-horizontal coupling. A matching tiltmeter to correct for this inevitable coupling is needed. Alternatively, the sensor should operate in a low tilt environment, for instance on a stage just above the test masses.

Future gravitational wave detectors need more sensitive inertial sensors to meet their low-frequency goals. In particular, the cryogenic Einstein Telescope [11] needs low-frequency inertial sensors to monitor the impact of their cryocoolers. They are linked via their own seismic attenuators to the stage just above the mirror to provide a heat sink to keep the mirror at design temperature. Therefore it is important to monitor if these systems operate according


Content from this work may be used under the terms of the Creative Commons Attribution 3.0 licence. Any further distribution of this work must maintain attribution to the author(s) and the title of the work, journal citation and DOI.
Published under licence by IOP Publishing Ltd

to design. The inertial sensors can additionally be deployed on the Moon and directly observe gravitational waves by detecting the Moon's response to passing waves [12].

Below, we describe a Cryogenic Superconducting Inertial Sensor (CSIS) which is an upgrade from said accelerometer [9] in section 2. Then we describe and show preliminary manufacturing results of the superconducting low-noise actuators in section 3. We end with the conclusion.

2. First application of our superconducting coils

A design and a description of CSIS are shown in figure 1. The mechanical part is a monolithic Watt's linkage, fabricated with the Electo-Discharge Machining (EDM). The monolithic design aim to avoid having separate mechanical parts which could cause thermal dissipation [8]. Niobium was the chosen material as it has a critical temperature $T_c = 9.2$ K, high strength and high intrinsic bulk quality factor [10]. Once machined as a Watt's linkage, a mechanical Q factor of 10^4 was estimated [13].

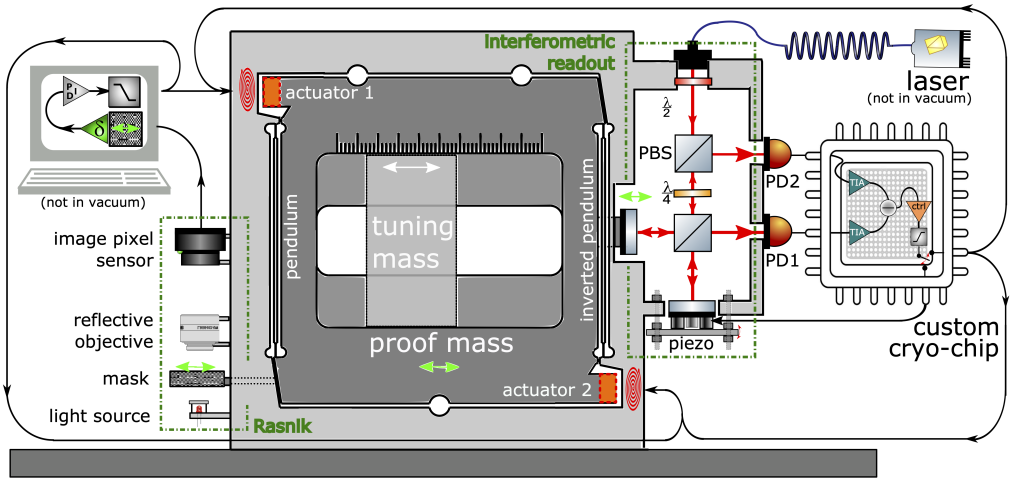

Figure 1. A Cryogenic Superconducting Inertial Sensor (CSIS). The proof mass is a 1 kg mass suspended by a Watt's linkage–a combination of a pendulum with an inverted pendulum–to lower the natural frequency, increasing the mechanical sensitivity. The position of the proof mass is probed by a long-range Rasnik [14] readout and interferometric readout system. The error signals provided by both readouts are used in a loop to lock the mass with respect to the frame using two actuators. These actuators generate a Meissner effect induced magnetic pressure on the superconducting surfaces of the proof mass.

The minimum detectable inertial displacement for CSIS is shown in figure 3. In this noise budget the suspension natural frequency was assumed to be 0.1 Hz. The niobium mechanics are fully superconducting below about 5 K, see [15] for the temperature dependence of superconducting properties of Nb from 3D to 2D films. If this sensor design is to be operated at higher temperatures, we can use high-T_c superconductors as doped cuprates or magnesium diboride. Typically, the mechanical performance of these materials is not sufficient to make a high-Q mechanical oscillator and, therefore, a hybrid solution can be pursued.

In figure 2 we present a fabrication method towards a Watt's linkage out of silicon. When carefully assembled, we expect a mechanical Q factor around 10^6. In this way, a material with an arbitrarily high T_c can be used for the coil as well as the surface–see orange rectangles in figure 1–attached to the proof mass.

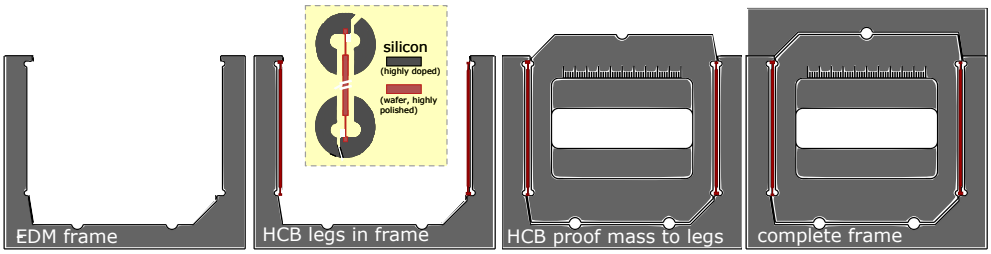

Figure 2. Assembly procedure for a low mechanical loss silicon Watt's linkage using Hydro-Catalysis Bonding (HCB). A frame–in 2 pieces–and proof mass is cut out of highly doped silicon block using spark erosion techniques, e.g. EDM. The leg and flexures are laser assisted plasma etched out of a thick 500 μm high-quality wafer.

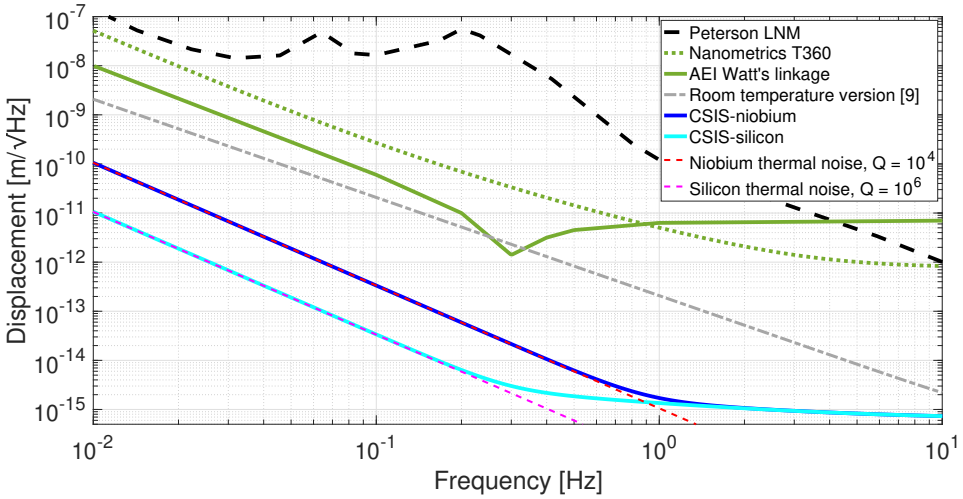

Figure 3. Displacement sensitivity of a niobium and silicon CSIS compared to the most sensitive seismic sensors available on the market and the room temperature interferometrically read out Watt's linkage. The CSIS noise budget is roughly shaped by the structurally damped thermal noise below 1 Hz and noise associated with the interferometric readout above 1 Hz at the level of fm/$\sqrt{\text{Hz}}$. The Peterson's Low Noise Model (LNM) [16] is additionally shown.

3. Low-noise superconducting spiral actuators

The low-noise actuator is a thin film of superconductive material deposited on a substrate and it has the shape of a spiral pancake. In the case of CSIS, a spiral coil will generate a magnetic field perpendicular to the actuator plane towards the proof mass, as shown in figure 4a. The geometry is an Archimedean 20-turn spiral with inner and outer diameter of 0.1 cm and 1.0 cm, respectively. The coil produces a push-only force on the proof mass surface and therefore two actuators per inertial sensor are necessary. This method will reduce mechanical losses by not using magnets, which greatly reduces viscous eddy current damping. Figure 4b shows the z-component of magnetic field, B_z, from a distance $z = 0.1$ mm of the coil when a stationary current of $I = 100$ mA is running through it, calculated with the Biot-Savart law. These results were verified by simulations using finite element analysis software.

The magnetic pressure is given by $p_{\text{mgn}} = B_z^2/(2\mu_0)$. Assuming an effective area of 1 cm^2 for the proof mass surface, the actuator force is about 1.7 μN. For a comparison, the Peterson high

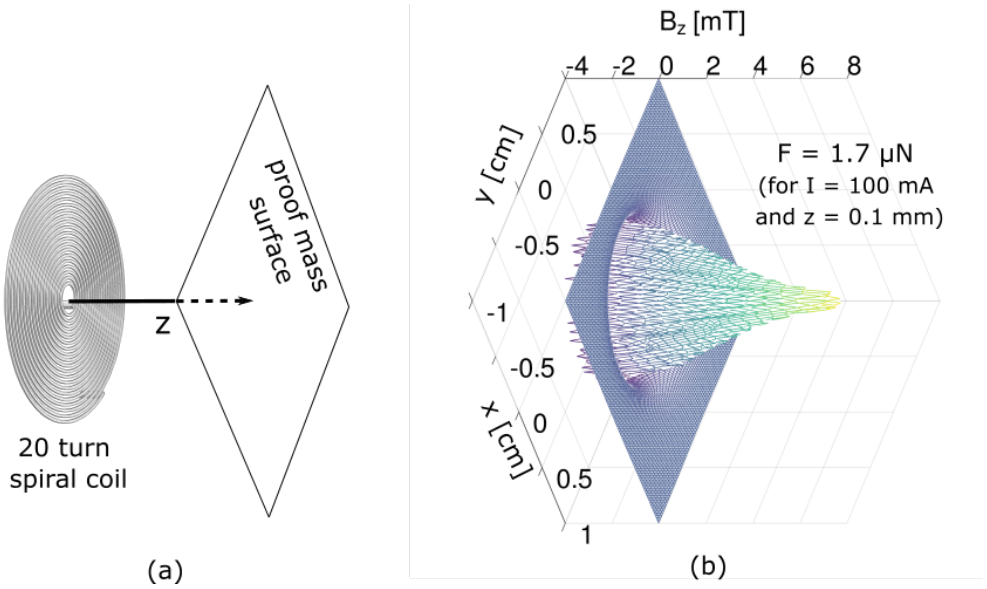

Figure 4. Superconducting spiral actuator for CSIS. (a) A scheme of the spiral coil placed at a distance z and perpendicular to the CSIS proof mass surface. (b) A plot of the z-component of the magnetic field applied to the proof mass surface when a current of 100 mA is running on the coil. The magnetic force, F, on the surface is a result of the Meissner effect.

noise model [16] peaks around 1.5 $\mu g\text{Hz}^{-1/2}$ which requires 15 μN $\text{Hz}^{-1/2}$ for a 1 kg proof mass. Therefore, the calculated force is enough because the motion at the penultimate stage of ET suspensions or on the lunar surface will be much lower. Additionally, the Rasnik loop will damp the mechanical amplification of the proof mass suspension and reduce the residual motion the interferometric readout loop has to cope with.

The maximum force applied by the actuator is limited by the minimal practical distance z, the maximum number of turns–governed by the deposition process–and maximum current limited in the driving CMOS cryo-chip to about 100 mA. To build the spiral geometry, a mask will be placed above the substrate during the deposition process. This produces a spiral strip of order 100 μm wide. Considering the geometrical section of the strips and the injected current, the obtained current density flowing in the spiral coil is well below the superconducting critical current density around 5 K [15]. Dissipation in Nb superconductors cannot be activated by vortex motion in such conditions.

Depositions of metallic thin films have been made on boron doped silicon (100) substrate without masks by magnetron sputtering. Not only niobium - that has a full Meissner state below 5 K and for the range of magnetic field intensities generated in the system - but also niobium nitrate (NbN) thin films were produced. In the cubic crystalline phase (δ), NbN has a higher $T_c \approx 16$ K than pure Nb [17] and full Meissner state below 9 K. Diffractograms of the Nb and NbN films were collected with CuKα radiation ($\lambda = 1.54184$ Å) from 5 to 100° 2θ angle (step size of 0.0167°) on a PANalytical diffractometer.

Figure 5 show diffractograms associated at Nb and NbN. Both seem to appear in a cubic phase (δ) with a preferential growth along the plane (111). The shift between theoretical (dotted lines) and measured angle of diffraction of peaks is associated to strain into the film. These results show that the films are in the correct crystalline phase to reach superconductivity at the expected temperatures.

The NbN thin film can be used to produce the actuators if the same material (or a material

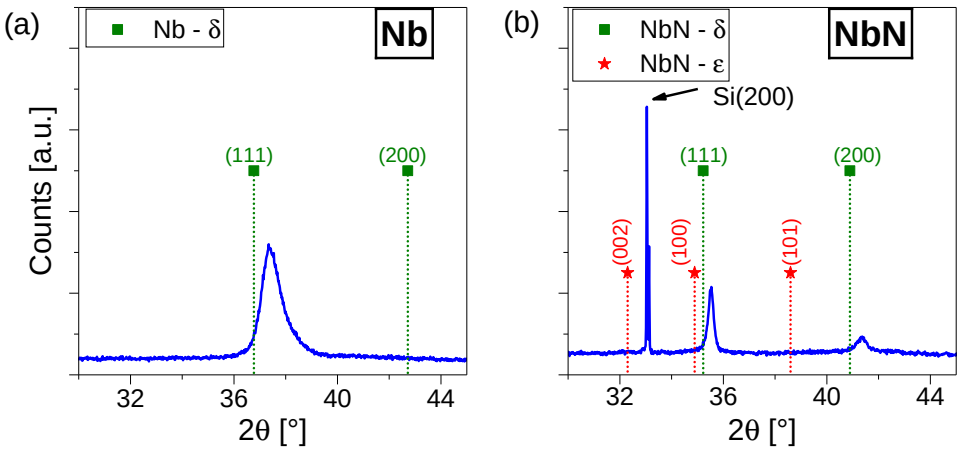

Figure 5. Diffractogram of (a) niobium film with theoretical value (dotted lines) and (b) niobium nitride film with theoretical values for δ and ϵ phases (dotted lines).

with equivalent T_c) is deposited on the surfaces of the proof mass facing the coils. The bulk material of CSIS can then for instance be changed to silicon, as discussed before.

4. Final remarks

A niobium Watt's linkage with a Rasnik and interferometric readout and the superconducting coils are under development. Deposition quality of strips and coil designs will first be assessed using cryogenic resistance and impedance measurements. Cryogenic force measurements are planned subsequently before installation in the inertial sensor prototypes. Next to Nb and NbN, creating the discussed structures using YBCO, with $T_c = 93\,\mathrm{K}$ or MgB_2, with $T_c = 40\,\mathrm{K}$, will also be explored. Different applications of the coil, for instance the control of the cryogenic part of the E-TEST suspension, are additionally investigated.

Acknowledgments

This work is funded by the BEWARE program of the Service Public de Wallonie under project SUNRISE (convention 2010245).

References

[1] Abbott B P *et al.* 2016 *Phys. Rev. Lett.* **116** 061102
[2] Abbott B P *et al.* 2017 *Phys. Rev. Lett.* **119** 161101
[3] Abbott B P *et al.* 2017 *ApJL* **484(2)** L12
[4] Kirchhoff R *et al.* 2017 *Rev. Sci. Instr.* **88** 115008
[5] Geotech Instruments LLC http://www.geoinstr.com/sensors.htm
[6] Ballardin G *et al.* 2001 *Rev. Sci. Instr.* **72** 3643
[7] Gray M B *et al.* 1999 *Opt. Quant. Electron.* **31** 571-582
[8] Bertolini A *et al.* 2006 *Nucl. Instr. and Meth.* **556** 616.
[9] van Heijningen J V *et al.* 2018 *IEEE SAS proceedings* 76-80
[10] Finnemore D K *et al.* 1966 *Phys. Rev.* **149** 231
[11] Punturo M *et al.* 2010 *Class. Quantum Grav.* **27** 194002.
[12] Harms J *et al.* 2021 *ApJ* **910** 1.
[13] van Heijningen J V 2020 *JINST* **15** P06034.
[14] van der Graaf H 2021 arXiv:**2104**.03601
[15] Pinto N *et al.* 2018 *Scientific Reports* **8** 4710.
[16] Peterson J 1993 *U.S. Department of Interior Geological Survey OFR* **93-322**
[17] Leith S *et al.* 2021 *Supercond. Sci. Technol.* **34** 025006.